arXiv:2005.06865v1 [physics.chem-ph] 14 May 2020

Refraction of fast Ne atoms in the attractive well of LiF(001) surface

M. Debiossac,[1] P. Roncin,[1] and A.G. Borisov[1]

[1]*Institut des Sciences Moléculaires d'Orsay (ISMO), UMR 8214 CNRS - Université Paris-Sud, Université Paris-Saclay, bât 520, Orsay, France*

(Dated: January 4, 2022)

Ne atoms with energies up to 3 keV are diffracted under grazing angles of incidence from a LiF(001) surface. For a small momentum component of the incident beam perpendicular to the surface, we observe an increase of the elastic rainbow angle together with a broadening of the inelastic scattering profile. We interpret these two effects as the refraction of the atomic wave in the attractive part of the surface potential. We use a fast, rigorous dynamical diffraction calculation to find a projectile-surface potential model that enables a quantitative reproduction of the experimental data for up to ten diffraction orders. This allows us to extract an attractive potential well depth of 10.4 meV. Our results set a benchmark for more refined surface potential models which include the weak Van der Waals region, a long-standing challenge in the study of atom-surface interactions.

Refraction is a well known phenomenon occurring when light is deflected at an interface between two transparent media of different refractive indices. In the early days of quantum mechanics, refraction of matter-wave was first observed with electrons [1, 2] and was explained by considering the beam to be refracted by the inner potential of the material [3]. Refraction has been also reported for neutrons [4]. For molecular and atomic projectiles scattered from surfaces at thermal energies [5, 6], the refraction is produced by an attractive Van der Waals (VdW) part of the projectile-surface interaction potential [7]. Thus, collision experiments between neutral atoms and surfaces represent an ideal platform for characterization of the physisorption region dominated by weak VdW polarisation forces [8, 9] which is of paramount importance for various practical applications [10–13].

So far atom scattering studies of the attractive part of the surface potential have been mostly performed using diffraction and refraction of the projectile beams at thermal energies [5, 9, 14, 15]. Recent observation of the surface diffraction of fast atoms of keV energies under grazing incidence (GIFAD or FAD) [16–18] offered yet unexplored possibilities of the surface analysis. Grazing incidence conditions imply slow motion of the projectile perpendicular to the surface during the fast motion parallel to it. GIFAD thus combines the sensitivity of thermal atoms with the geometry of reflection high energy electron diffraction, that allows one to record the full diffraction pattern at once using an imaging detector (Fig.1). Fast atom diffraction has already proven to be sensitive to surface rumpling at the pm scale [19] and to the VdW potential [20, 21], in particular with the observation of bound state resonances [22]. Similar to the thermal atom diffraction, most of the GIFAD studies have been performed with light (He, H, H_2) projectiles. The diffraction experiments with heavier Ne atoms are challenging because of enhanced sensitivity to defects [14, 23–26]. Nevertheless, distinct quantum feature as supernumerary rainbows were measured [27, 28] suggesting that high coherence elastic diffraction could be observed.

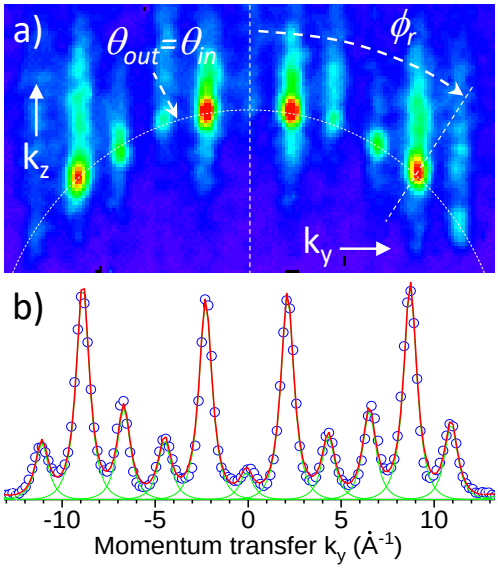


FIG. 1: a) Diffraction pattern in the (k_y, k_z) plane recorded for 500 eV Ne atoms scattered off LiF(001) surface along the ⟨110⟩ direction. The Laue circle is shown with a dashed white line and corresponds to an grazing incidence angle $\theta = 0.33°$. ϕ_r indicates the classical rainbow angle. b) Projected experimental intensity along the Laue circle (blue circles). The red line corresponds to a fit of the diffracted intensity using a single empirical Lorentzian line-shape for all peak (green line).

In this Letter we show well-resolved elastic diffraction of fast Ne atoms on a LiF surface. We fully exploit the shorter wavelength of Ne atoms so that many diffraction peaks can be observed offering a surface probe with a resolution not obtainable with light projectiles [29]. In particular, we reveal the refraction of the matter wave at the surface resulting in a shift of the elastic rainbow angle, and the broadening of the inelastic profile. Rich diffraction patterns measured in our experiments provide further insights on the projectile-surface interaction from a detailed comparison with quantum simulation. Our work, provides an important basis for a characterization

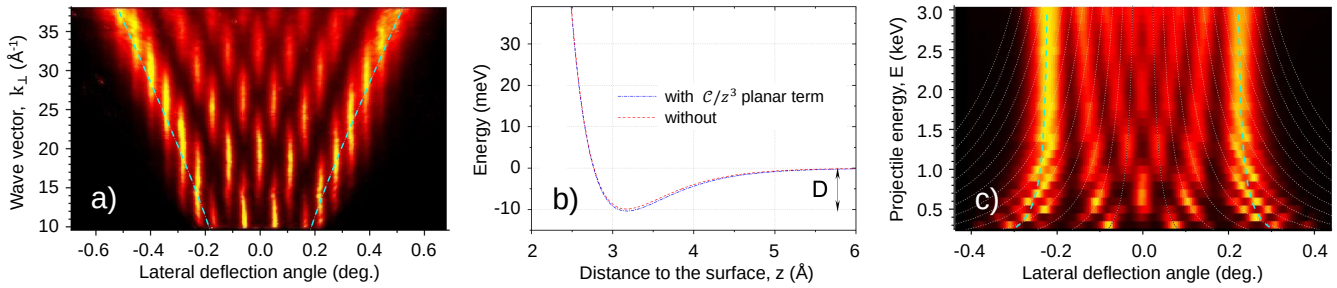


FIG. 2: a) Experimental diffraction chart for 500 eV Ne atoms scattered off LiF(001) surface along the ⟨110⟩ direction. The grazing incidence angle θ is varied between 0.27° and 0.95°. The intensity of the diffraction orders is shown as function of the lateral deflection angle, α, and $k_\perp$ the momentum component of the incident beam perpendicular to the surface. b) Theoretical planar potential $V(z)$ as a function of the distance z from the LiF surface. The blue (red) line corresponds to the calculation with (without) an explicit planar attractive term. D indicates the potential well depth. c) Same as a), but for the fixed incidence angle $\theta = 0.42°$ and total kinetic energy E varied in $0.3-3$ keV range. The intensity of the diffraction orders is shown as function of the lateral deflection angle α and beam energy E. The white dotted lines follow the position of the diffraction orders. The blue dashed line in panels a) and c) indicates the position of the rainbow angle calculated from Eq. (1) using $D = 10$ meV.

of the physisorption region for heavy atomic projectiles, which is a challenge both experimentally and theoretically.

A typical diffraction image is displayed in Fig. 1. The LiF(001) surface corresponds to the (x, y)-plane, and Ne projectiles are incident under grazing incidence angle θ measured in the (x, z) specular plane. The bright spots located on the Laue circle of energy conservation are due to elastic diffraction, whereas inelastic diffraction leads to the elongated streaks [30, 31]. In Fig. 1 the rainbow angle is denoted as ϕ_r. Within the classical picture it corresponds to the largest angular deflection of the incident beam. In the quantum diffraction pattern, it is associated with intense diffraction spots at maximum lateral deflection. For the GIFAD scattering conditions, the axial surface channeling approximation (ASCA) [17, 32–34] provides a powerful framework for the data analysis that we will use here. Within ASCA the fast motion along x-direction and the slow motion in the (y, z)-plane perpendicular to the surface are decoupled. When the x-direction coincides with a surface crystal axis, the elastic diffraction pattern such as observed in Fig. 1, is equivalent to that of a projectile with a wave-vector $k_\perp = k \sin\theta$ and energy $E_\perp$, incident at the potential $V_{2D}(y, z)$. Here, $k = \sqrt{2ME}$ is the total momentum, E is the energy of the beam so that $E_\perp = E \sin^2\theta$, M is the projectile mass, and $V_{2D}(y, z)$ is the total projectile-surface interaction potential $V(x, y, z)$ averaged along x.

Prior to discussion of the experimental evidence of refraction effects we find it useful to use the ASCA and to introduce a simple and intuitive model as a guide to understand the main results of this work.

Consider the projectile-surface collision as a three step process (i) acceleration by an attractive VdW interaction on the ingoing path; (ii) collision with the surface leading to the deflection by the $V_{2D}(y, z)$ potential; (iii) deceleration by the VdW interaction on the outgoing path. Within this scenario, the largest lateral momentum resulting from the scattering with the surface is $k_y = \sqrt{k_\perp^2 + 2MD}\ \sin\tilde{\phi}_r$. Here, D accounts for the acceleration on the ingoing path, and $\tilde{\phi}_r$ is the "true" rainbow angle given by the fastest variation of $V_{2D}(y, z)$ with y [35]. The associated maximum lateral deflection angle α, and the rainbow angle ϕ_r "observed" in the outgoing beam are defined with $\sin\alpha = k_y/k$, and $\sin\phi_r = k_y/k_\perp$. We then obtain

$$\sin\alpha = \sin\phi_r \sin\theta = \sin\tilde{\phi}_r\ \sin\theta \sqrt{1 + \frac{D}{E_\perp}}. \quad (1)$$

It follows from Eq. (1) that for the incidence conditions such that $E_\perp$ becomes comparable with the depth of the attractive potential well D, the refraction effects strongly alter the observed rainbow and maximum lateral deflection angles. If the energy of the beam E is fixed, decreasing the grazing incidence angle θ leads to α that tends to a constant non-zero value. This is in complete contrast with the $\alpha = 0$ limit (pure specular reflection) that would be expected in the absence of the projectile attraction to the surface. Similarly, if the angle θ is constant, decreasing the beam energy E leads to increasing deflection α, whereas it would be constant without VdW attraction.

We first demonstrate the refractive effects by analyzing the elastic intensity. Fig. 2a displays the diffraction chart obtained by varying the grazing incidence angle θ, for a fixed energy E of the incident beam. Here the radius of the Laue circle is proportional to θ while the angular distance $\Delta\alpha = G_y/k$ between diffraction orders stays constant. The reciprocal lattice vector of the LiF(001) surface is given by $G_y = 2\sqrt{2}\ \pi/a$ where $a = 4.03$ Å is the LiF lattice constant. The intensity of the diffraction orders oscillate with $k_\perp$, reflecting the interference of trajectories from the top and bottom of the corruga-

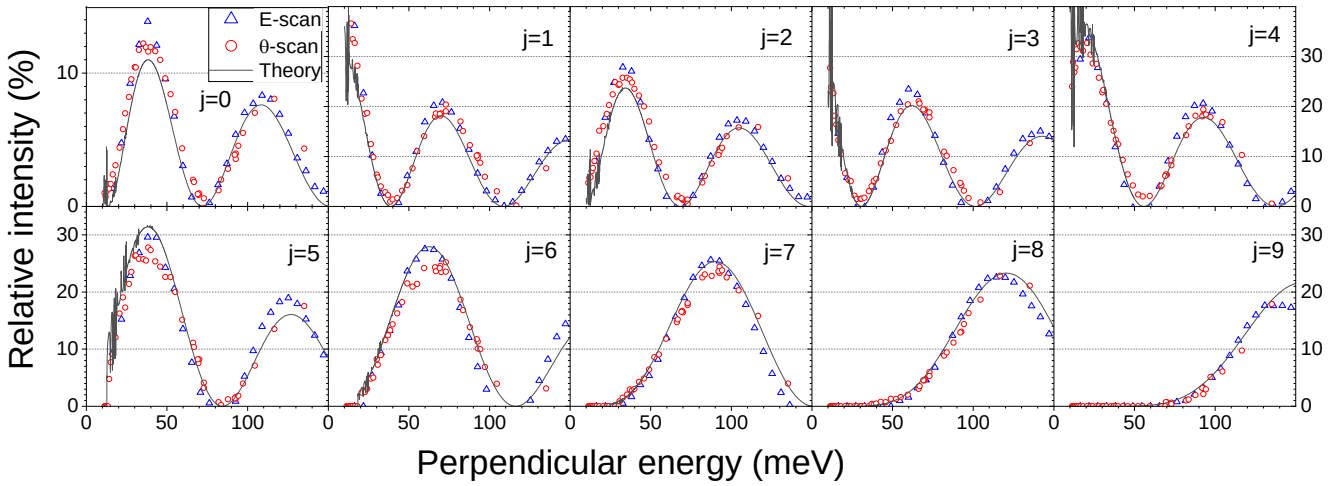


FIG. 3: Rocking curves for Ne atoms scattered along the ⟨110⟩ direction. The intensity of the j^{th} diffracted beam is shown as function of $E_\perp$, the energy of the motion in the (y,z)-plane. For the degenerate $\pm j$ diffraction orders, the summed intensity is shown. Diffracted intensities measured during a scan of the projectile energy (blue triangles) or grazing incidence angle (red circles), the black line is for theoretical results. The very narrow peaks calculated at low energies reveal the bound state resonances.

tion function. The general shape made of maxima aligned along nested V structures comes from the modulation of the intensity due to supernumerary rainbows. The outermost structure corresponds to the classical rainbow angle [27] measured here as $\phi_r = 31°$ in good agreement with earlier results [28]. At the lowest incidence angles θ (lowest $k_\perp$) the $\alpha(\theta)$-dependence of the maximum deflection angle and thus of the rainbow angle departs from linear, *inline* with the refraction effect described by Eq. (1).

Fig. 2c shows the diffraction chart obtained for different experimental conditions. Now, the grazing incidence angle θ is fixed while the total energy E is varied. In this situation, the difference in Bragg angles separating adjacent diffraction orders changes as $\Delta\alpha = G_y/\sqrt{2ME}$ (see white dotted lines in Fig.2c). The maximum deflection angle α as well as the rainbow angle ϕ_r is constant for energies above 1.5 keV [28]. At smaller energies α and so ϕ_r increases with decreasing E. This effect is often interpreted as being due to a larger "effective" surface corrugation [35]. However, such an explanation does not hold here as follows from the calculated atom-surface interaction potential. Instead, the observed trends stem from the refraction of Ne atoms in the attractive VdW potential. This conclusion is supported by the comparison between the measured projectile energy dependence of the rainbow structure in the experimental diffraction chart, and $\alpha(E)$-dependence calculated with Eq. (1).

In order to obtain further insights into the Ne interaction with LiF(001) surface we have performed a dynamical diffraction theory study within the ASCA approximation. The wave function of Ne projectile is given in the form $\Psi(y,z) = \sum_j \psi_j(z) e^{ijG_y}\sqrt{(2\pi/G_y)}$ leading to the set of close-coupling equations [36] for diffraction orders j.

$$-\frac{1}{2M}\left[\frac{\partial^2}{\partial z^2} - (jG_y)^2\right]\psi_j + \sum_\ell W_{j\ell}\psi_\ell = E_\perp \psi_j(z). \quad (2)$$

Solving Eq. (2) leads to the extraction of the scattering matrix [37] and thus of the intensities of the diffracted beams. The coupling matrix $W_{j\ell}$ is given by

$$W_{j\ell}(z) = \int_{-L/2}^{L/2} dx \int_{-L/2}^{L/2} dy\; V(x,y,z)\;\frac{e^{i(\ell-j)Gy}}{L}. \quad (3)$$

The Ne-surface interaction potential is searched in a form comprising both planar and binary interaction terms

$$V(\mathbf{r}) = -\mathcal{C}/z^3 + \sum_{n=1,2}\frac{a_{n,s}}{|\mathbf{R}_s - \mathbf{r}|}e^{-\gamma_{n,s}|\mathbf{R}_s-\mathbf{r}|}, \quad (4)$$

where $\mathbf{r} = (x,y,z)$, and the sum runs over the $s = \mathrm{Li, F}$ lattice sites located at $\mathbf{R}_s$. For the planar attractive VdW interaction $-\mathcal{C}/z^3$[9], the $z = 0$ is set at the plane of surface F^- ions. The second term in Eq. 4 is a sum of screened coulomb binary interaction potentials. These forms decay exponentially at large distances and have proven their efficiency in atom-atom scattering in general [38] and also in reproducing GIFAD data for various systems [27, 35]. We have also accounted for the rumpling of −0.05 Å[19] in position of surface Li atoms with respect to the LiF(001) surface plane.

Representation given by Eq. (4) allows an analytical closed-form expression for the coupling matrix so that the diffraction chart can be calculated in seconds allowing on-the-fly optimization of the potential. Here the $\mathcal{C}, a_{n,s}, \gamma_{n,s}$ starting parameters were derived from the

binary potentials deduced in [39] from the density functional theory DFT calculations of the Ne / LiF(001) interaction. The intensities of the diffracted beams as function of $E_\perp$, derived by solving equations Eq. (2) are compared with experimental values for the energies $E_\perp$, between 20 and 150 meV. The potential parameters are then optimized using a least squares minimization.

Figure 3 shows an excellent agreement with the data over the complete energy range. The $\mathcal{C}, a_{n,s}, \gamma_{n,s}$ parameters extracted here are reported in Ref [40]. Below 20 meV, the theory indicates numerous narrow peaks associated with bound state resonances. To avoid singular behavior, this energy range was not included in the fit.

The planar potential $V(z)$ deduced from our fit is shown in Fig. 2b. It is characterized by a $D = 10.4$ meV attractive potential well, in good agreement with thermal atom diffraction data [9, 41, 42]. Note that a higher value D = 13.5 meV has been also reported [14] based on observation and modeling of bound state resonance but the difficult line assignment has never been confirmed. With our parametrization, the attractive well is obtained owing to both the $\mathcal{C}/z^3$ term and the attractive part of the binary interaction potentials. To further test the robust character of our surface potential model, we performed another potential optimisation imposing $\mathcal{C} = 0$. In this situation the attraction to the surface is entirely given by the negative terms ($a_n < 0$) of the binary potentials. Our fit also reported in Ref [40] and displayed in Fig. 2b) then indicates a value $D = 9.9$ meV, very close to $D = 10.4$ meV reported above. We have also tried to use the binary potentials derived in Ref [35, 38] but the convergence is much slower in spite of having twice as many terms in the expansion (n=4) in Eq. 4. This highlights that extrapolation is a difficult task, Z.B.L. interaction potentials [38] optimized to fit scattering of keV to MeV projectiles at quasi-normal incidence were found too repulsive when probing rainbow angles at grazing incidence with $E_\perp$ in the 0.1 eV-50 eV range [27, 35]. For $E_\perp$ between 20 and 150 meV, our study indicates that both Ref [35, 38] underestimate the attractive potential responsible for physisorption well, which is the main focus of this work.

Another evidence for refraction of Ne atoms is provided by the analysis of the *inelastic* polar scattering profile. It is obtained from the experimental data by subtracting the sharp peaks of the elastic contribution on the Laue circle [30] (see *e.g.* Fig. 1). The inset in Fig.4 shows that the resulting intensity distribution over polar exit angles $P(\theta_{out})$ is well fitted by a log-normal profile [30, 31] allowing its width σ_θ to be define. Fig. 4 shows a clear increase of σ_θ with decreasing $E_\perp$. This is despite the Ne atoms interacting less strongly with the surface. This apparent contradiction can be understood from the simple scattering model outlined at the beginning. For simplicity we consider only the scattering in the specular plane (x, z). In our experimental conditions the distance

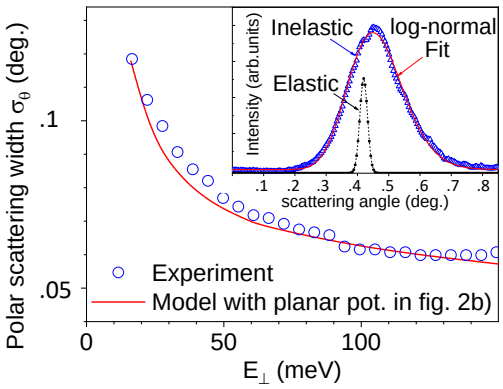


FIG. 4: The width σ_θ of the polar inelastic scattering profile. Dots (line) show the experimental (model) results as a function of the energy of the motion in the (y, z)-plane, $E_\perp$. The inelastic profile is obtained from experimental data by subtracting the elastic contribution. σ_θ is extracted from the inelastic profile using a log-normal fit as shown in the insert for 500 eV neon at 0.42 deg.

of closest approach to the surface amounts to few Åand is much larger than the amplitude of thermal motion of the surface atoms σ. A perturbative approach then predicts a log-normal scattering profile with a relative angular width $\sigma_{\tilde{\theta}}/\tilde{\theta} \propto \Gamma\sigma$ [31, 32]. Here Γ is the logarithmic derivative of the interaction potential between the Ne atom and the surface evaluated at the turning point of the trajectory. The "effective" polar scattering angle $\tilde{\theta}$ and the "observed" polar scattering angle θ are related as $\tilde{\theta}^2 = \sqrt{\theta^2 + D/E}$ so that, for small angular broadening we obtain $d\tilde{\theta} = d\theta/\sqrt{1 + D/E_\perp}$. While $\sigma_{\tilde{\theta}}$ is fixed by the scattering conditions in the vicinity of the surface, the observed polar angle width σ_θ increases with decreasing $E_\perp$. The proportionality factor between σ_θ and Γ is adjusted at $E_\perp$= 120 meV and the model displayed in Fig. 4 reproduces qualitatively well the drastic increase at low energy.

In conclusion, we reported well resolved elastic diffraction of neon atoms from LiF(001) surface. Combined with a fast algorithm using dynamical diffraction theory, the large number of diffraction orders observed experimentally with these heavy projectiles allows a refinement of the model projectile-surface interaction potential. The quantitative agreement reached between the theory and experiment is remarkable and its sensitivity to the potential parameters yields a robust estimate of the depth of the attractive van der Waals potential well. Our work also sheds light on the analogies between geometrical optics and projectile scattering at surfaces, where the refraction of atomic beams manifests itself via the significant increase of the elastic azimuthal rainbow angle as well as via the drastic increase of the polar inelastic scattering profile. Even in the absence of observation of any bound states resonances, the accurate determi-

nation of the diffracted intensities at grazing incidence conditions is a powerful strategy to measure the van der Waals forces needed to refine *ab initio* theoretical descriptions. In this energy range, neon atoms offer an increased sensitivity owing to their shorter wavelength and even inelastic effects contribute to an accurate self-consistent determination of attractive forces. Further investigations are needed to develop a quantitative theory for inelastic diffraction of fast atoms supporting our interpretation of the inelastic scattering profiles.

ACKNOWLEDGMENT

J.E. Miraglia and M.S. Gravielle are kindly acknowledged for providing a compact form of their results [39].

[1] C. Davisson and L. Germer, Proceedings of the National Academy of Sciences of the United States of America **14**, 619 (1928).

[2] S. Nishikawa and S. Kikuchi, Nature **122**, 726 (1928).

[3] T. Yamaguti, Proceedings of the Physico-Mathematical Society of Japan. 3rd Series **12**, 203 (1930).

[4] A. G. Klein and S. A. Werner, Reports on Progress in Physics **46**, 259 (1983).

[5] J. Harris, A. Liebsch, G. Comsa, G. Mechtersheimer, B. Poelsema, and S. Tomoda, Surface Science **118**, 279 (1982), ISSN 0039-6028.

[6] B. S. Zhao, G. Meijer, and W. Schöllkopf, Science **331**, 892 (2011).

[7] J. L. Beeby, Journal of Physics C: Solid State Physics **4**, L359 (1971).

[8] D. Farías and K. Rieder, Reports on Progress in Physics **61**, 1575 (1998).

[9] H. Hoinkes, Rev. Mod. Phys. **52**, 933 (1980).

[10] A. Kühnle, Current Opinion in Colloid and Interface Science **14**, 157 (2009).

[11] Y. Andersson, E. Hult, H. Rydberg, P. Apell, B. I. Lundqvist, and D. C. Langreth, *Van der Waals Interactions in Density Functional Theory* (Springer US, Boston, MA, 1998), pp. 243–260.

[12] M. Nijkamp, J. Raaymakers, A. van Dillen, and K. Jong, Applied Physics A **72**, 619 (2001).

[13] S. D. Feyter, A. Gesquière, M. Abdel-Mottaleb, P. Grim, F. C. D. Schryver, C. Meiners, M. Sieffert, S.Valiyaveettil, and K. Müllen, Accounts of Chemical Research **33**, 520 (2000).

[14] E. Semerad, P. Sequard-Base, and E. Hrl, Surface Science **189-190**, 975 (1987).

[15] J. G. Mantovani and J. R. Manson, Surface Science **120**, L487 (1982).

[16] A. Schüller, S. Wethekam, and H. Winter, Phys. Rev. Lett. **98**, 016103 (2007).

[17] P. Rousseau, H. Khemliche, A. G. Borisov, and P. Roncin, Phys. Rev. Lett. **98**, 016104 (2007).

[18] H. Winter and A. Schller, Progress in Surface Science **86**, 169 (2011), ISSN 0079-6816.

[19] A. Schüller, S. Wethekam, D. Blauth, H. Winter, F. Aigner, N. Simonović, B. Solleder, J. Burgdörfer, and L. Wirtz, Phys. Rev. A **82**, 062902 (2010).

[20] M. Debiossac, A. Zugarramurdi, H. Khemliche, P. Roncin, A. G. Borisov, A. Momeni, P. Atkinson, M. Eddrief, F. Finocchi, and V. H. Etgens, Phys. Rev. B **90**, 155308 (2014).

[21] M. Debiossac, A. Zugarramurdi, Z. Mu, P. Lunca-Popa, A. J. Mayne, and P. Roncin, Phys. Rev. B **94**, 205403 (2016).

[22] M. Debiossac, A. Zugarramurdi, P. Lunca-Popa, A. Momeni, H. Khemliche, A. G. Borisov, and P. Roncin, Phys. Rev. Lett. **112**, 023203 (2014).

[23] K. Rieder, Surface Review and Letters **1**, 51 (1994).

[24] A. Al Taleb, G. Anemone, W. W. Hayes, J. R. Manson, and D. Farías, Phys. Rev. B **95**, 075414 (2017).

[25] K. J. Nihill, J. D. Graham, and S. J. Sibener, Phys. Rev. Lett. **119**, 176001 (2017).

[26] G. Anemone, A. Al Taleb, W. W. Hayes, J. R. Manson, and D. Farías, The Journal of Physical Chemistry C **121**, 22815 (2017).

[27] A. Schüller and H. Winter, Phys. Rev. Lett. **100**, 097602 (2008).

[28] M. Gravielle, A. Schller, H. Winter, and J. Miraglia, NIM–B **269**, 1208 (2011).

[29] K. H. Rieder and W. Stocker, Phys. Rev. Lett. **52**, 352 (1984).

[30] M. Debiossac and P. Roncin, NIM–B **382**, 36 (2016).

[31] P. Roncin and M. Debiossac, Phys. Rev. B **96**, 035415 (2017).

[32] J. R. Manson, H. Khemliche, and P. Roncin, Phys. Rev. B **78**, 155408 (2008).

[33] A. Zugarramurdi and A. G. Borisov, Phys. Rev. A **86**, 062903 (2012).

[34] A. Muzas, F. Gatti, F. Martn, and C. Daz, NIM–B **382**, 49 (2016).

[35] A. Schller, K. Grtner, and H. Winter, EPL (Europhysics Letters) **81**, 37007 (2008).

[36] J. R. Manson, *Theoretical Aspects of Atom-Surface Scattering* (Springer-Verlag, Berlin, Heidelberg, 2013), pp. 173–205, ISBN 0931-5195.

[37] D. W. Norcross and M. J. Seaton, Journal of Physics B: Atomic and Molecular Physics **6**, 614 (1973).

[38] J. F. Ziegler and J. P. Biersack, *The Stopping and Range of Ions in Matter* (Springer US, Boston, MA, 1985), pp. 93–129, ISBN 978-1-4615-8103-1.

[39] J. E. Miraglia and M. S. Gravielle, Phys. Rev. A **95**, 022710 (2017).

[40] All values are given in atomic units. Fit parameters for the potential *with* planar VdW term: ($a_{1,F}$ = 74.7578, $\gamma_{1,F}$ = 1.6108); ($a_{2,F}$ = −1.4581, $\gamma_{2,F}$ = 0.9940); ($a_{1,Li}$ = 23.0115, $\gamma_{1,Li}$ = 1.9288); ($a_{2,Li}$ = −1.8785, $\gamma_{2,Li}$ = 1.2149); $\mathcal{C} = 3.6052 \times 10^{-3}$. Fit parameters for the potential *without* planar VdW term: ($a_{1,F}$ = 79.5900, $\gamma_{1,F}$ = 1.6364); ($a_{2,F}$ = −1.6632, $\gamma_{2,F}$ = 1.0165); ($a_{1,Li}$ = 39.8449, $\gamma_{1,Li}$ = 2.1082); ($a_{2,Li}$ = −1.6984, $\gamma_{2,Li}$ = 1.2465); $\mathcal{C} = 0$.

[41] G. Boato, P. Cantini, and L. Mattera, Surface Science **55**, 141 (1976), ISSN 0039-6028.

[42] G. Vidali, G. Ihm, H.-Y. Kim, and M. W. Cole, Surface Science Reports **12**, 135 (1991), ISSN 0167-5729.